PAPER

The transfer hydrogenation of high concentration levulinic acid to γ-valerolactone catalyzed by glucose phosphate carbamide zirconium†

Feifei Wan, Bo Yang, Jiekun Zhu, Dabo Jiang, Huanhuan Zhang, Qiao Zhang, Shuainan Chen, Chao Zhang, [ID] Yachun Liu and Zaihui Fu [ID] *

Zr-Based catalysts have been extensively applied in Meerwein–Ponndorf–Verley type catalytic transfer hydrogenation (CTH) reactions, but they are easily deactivated in the CTH conversion of high concentrations of levulinic acid (LA) to γ-valerolactone (γ-GVL). This work discloses that by using cheap glucose and ZrCl₄ as two main raw materials, glucose phosphate carbamide zirconium (GluPC-Zr) is easily synthesized at large scale and low cost *via* a simple two-step conversion. The constructed GluPC-Zr has enhanced Lewis acid–base properties and good porosity, thus exhibiting outstanding activity for the CTH reactions of LA or its esters with isopropanol (IPA), providing 95–98% γ-GVL yields. Because of the excellent esterification performance of the introduced acidic phosphate groups, GluPC-Zr also works well at high LA concentrations, achieving a much higher turnover frequency (TOF, 8.2 mmol γ-GVL per g catalyst per h) than previously reported Zr-based catalysts (TOF, 0.2–2.4). And it shows excellent reusability in the reaction of LA with IPA, still providing *ca.* 95% γ-GVL yield after the seventh cycle run. This work provides a preferential esterification strategy for LA to hamper catalyst deactivation, which is of special significance for the large-scale production of γ-GVL from biomass-derived LA and a low-cost GluPC-Zr catalyst.

1. Introduction

The over-exploitation and consumption of non-renewable fossil energy by the traditional chemical industry has been leading to an intensified energy crisis, global warming and severe environmental pollution, and the excessive consumption of fossil fuels and its impact on the greenhouse gas emissions into the environment highlights the need to explore renewable and green energy sources.[1,2] As we all know, lignocellulosic biomass is considered to be an abundant renewable resource[3] and it can be converted into high value-added platform chemicals, such as succinic acid, sorbitol,[4] and glycerol,[5–12] furfural,[13] 5-hydroxymethylfurfural,[14–18] levulinic acid,[19] and γ-valerolactone (γ-GVL).[20,21] Among the above biomass-derived platform chemicals, γ-GVL is acknowledged as a potential building block for the production of biofuels, biochemicals and polymeric materials,[22–25] and as a solvent,

National & Local United Engineering Laboratory for New Petrochemical Materials & Fine Utilization of Resources, Key Laboratory of Resource Fine-Processing and advanced materials of Hunan Province and Key Laboratory of Chemical Biology and Traditional Chinese Medicine Research (Ministry of Education of China), College of Chemistry and Chemical Engineering, Hunan Normal University, Changsha 410081, China. E-mail: fzhhnnu@126.com

†Electronic supplementary information (ESI) available. See DOI: 10.1039/d1gc00209k

food additive and flavoring agent.[26,27] γ-GVL can be synthesized by hydrogenation or Meerwein–Ponndorf–Verley type catalytic transfer hydrogenation (CTH) and then lactonization of another biomass-derived levulinic acid (LA) and its esters (LEs) with various hydrogen sources. The molecular H₂-involved conversion of LA and LEs to γ-GVL has a high hydrogenation efficiency in the presence of various transition metal catalysts and an almost quantitative γ-GVL yield can be achieved with precious metal catalysts, such as Ru, Ir, Pt, Pd and Au under heterogeneous[28–38] and especially homogeneous systems.[39–43] However, the high cost and scarcity of precious metals restrict their practical applications. In addition, high-pressure molecular hydrogen is normally required to improve γ-GVL yield with transition metal catalysts, which involves some problems, such as hydrogen transportation and storage.[44] To overcome these obstacles, multiple efforts have been devoted to eliminating reliance on external H₂. For example, formic acid (FA) has been adopted as a hydrogen source owing to its co-production with LA during the acid-promoted degradation of carbohydrates. FA can *in-situ* generate H₂ for the hydrogenation of LA by its decomposition over metal catalysts,[30,35,43,45] but precious metals and/or harsh conditions are still required to carry out the decomposition and hydrogenation steps and the leaching and/or sintering of metals during the reaction can also easily occur upon those inexpensive transition metal-containing catalysts.[46,47] For the

large-scale production of γ-GVL, catalytic schemes are required to maximize product yield without the use of precious metals, high H_2 pressure, or an excessive number of unit operations.[21] The δ-carbonyl of LA and LEs can be reduced to hydroxyl through the CTH reaction, which is conducted in H-donor solvents such as IPA or 2-butanol. This CTH reaction can achieve an almost quantitative γ-GVL yield but also provides an attractive alternative for ensuring the hydrogenation becomes inherently safe and environmentally friendly. Many catalysts exhibit high catalytic capability for the CTH reaction of LA with IPA[48,49] and some representative Zr-based catalysts listed in Table 1 can achieve *ca.* 88–97% γ-GVL yield and 0.2–2.4 turnover frequency (TOF, mmol γ-GVL per g catalyst per h) with 0.05–0.25 M LA in a batch reactor.[50–57] Moreover, the flow CTH reaction of 0.05 M LA dilute solution in IPA has been realized in a fixed bed reactor filled with Zr modified β zeolite particles, affording a stable 90% γ-GVL yield during continuous running (see Table 1).[58] However, the large-scale production of γ-GVL by the CTH pathway still needs to overcome the high catalyst cost, energy consumption and especially low production efficiency caused by the appreciable deactivation of Zr-based catalysts at high concentrations of LA.[59]

Two pathways have been reported to achieve the CTH reaction of LA with IPA.[60,61] One pathway is that the δ-carbonyl of LA is directly reduced by IPA to hydroxyl. Another pathway is that in the presence of IPA, the carboxyl of LA is first esterified and then its δ-carbonyl is reduced to hydroxyl (Scheme 1). It is expected that when the Zr-based catalyst simultaneously possesses excellent esterification and transfer hydrogenation activities, it should efficiently catalyze the conversion of a higher LA concentration to γ-GVL through the second CTH pathway. In order to develop this kind of catalyst, herein, we report that a new glucose phosphate carbamide-coordinated Zr catalyst (GluPC-Zr) prepared using cheap glucose and $ZrCl_4$ as two main raw materials can well achieve the CTH conversion of a high concentration of LA to γ-GVL.

2. Experimental section

2.1. Reagents and materials

The main reagents used in this work were of analytical grade, including glucose (Glu, >99.5%), phosphoric acid (H_3PO_4, 85%), urea (>99.0%), $ZrCl_4$ (>99.0%), levulinic acid (LA, 98.0%), methyl levulinate (ML, 99.0%), ethyl levulinate (EL,

Table 1 The conversion of LA to γ-GVL using IPA as an H-donor over Zr-based catalysts

Entry	Catalyst	Reaction conditions	γ-GVL yield (%)	TOF[a]	Ref.
1	Zr-PhyA (phytic acid)	0.25 M LA in IPA: 4 mL, 0.2 g of catalyst, 130 °C, 2 h	96.7	2.4	50
2	Zr-HA (humic acids)	0.20 M LA in IPA: 5 mL, 0.2 g of catalyst, 150 °C, 24 h	88.3	0.2	51
3	UiO-66-Zr	0.13 M LA in IPA: 30.55 mL, 0.8 g of catalyst, 0.24 g of naphthalene, 200 °C, 2 h	92.7	2.3	52
4	Zr-CA (cyanuric acid)	0.13 M LA in IPA: 7.64 mL, 0.2 g of catalyst, 130 °C, 4 h	96.8	1.2	53
5	Zr-TMPA (trimetaphosphate)	0.20 M LA in IPA: 5 mL, 0.2 g of catalyst, 160 °C, 8 h	96.2	0.6	54
6	Zr-HBA (hydroxyl benzoic acid)	0.13 M LA in IPA: 7.64 mL, 0.2 g of catalyst, 150 °C, 4 h	94.4	1.2	55
7	ZrF MOFs	0.05 M LA in IPA: 9.95 mL, 0.1 g of catalyst, 1 MPa N_2, 200 °C, 2 h	94	2.3	56
8	Organic Zr phosphonate	0.20 M LA in IPA: 4.9 mL, 0.2 g of catalyst, 160 °C, 12 h	95	0.4	57
9	Zr–Al-beta zeolite	0.05 M LA in IPA, feed flow rate: 0.05 mL min^{-1}, contact time: 5 min g mL^{-1}, 0.25 g of catalyst, 170 °C	90	3.4[b]	58
10	GluPC-Zr	1.87 M LA in IPA: 2.67 mL, 0.05 g of catalyst, 180 °C/190 °C, 12 h	95/98.1	7.9/8.2	This work

[a] Turnover frequency calculated based on the γ-GVL yield (mmol γ-GVL per g catalyst per h). [b] Productivity calculated based on the γ-GVL yield (g γ-GVL per g catalyst per h).
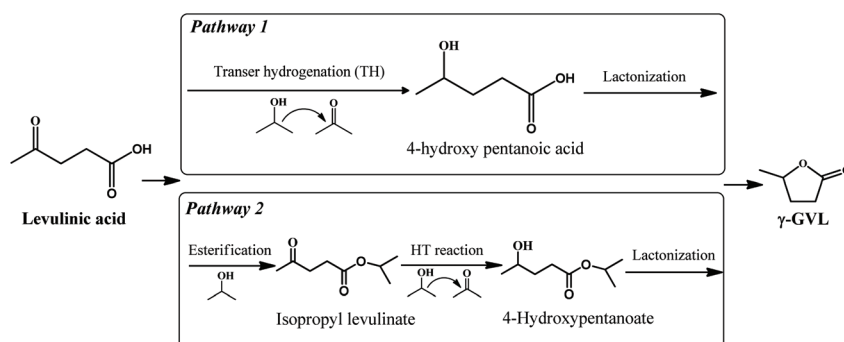
Scheme 1 The reaction pathways for synthesis of γ-GVL from LA with IPA over a Zr-based catalyst.

99.0%), isopropyl levulinate (IPL, 99%), butyl levulinate (BL, 99%), methanol (>99.5%), ethanol (>99.5%), propanol (>99.0%), 2-propanol (IPA, >99.0%), 2-butanol (>99.0%), cyclohexanol (>99%), ZrO_2 (>99.0%), $ZrOCl_2 \cdot 8H_2O$ (>99.0%), dodecane (98.0%). All chemical reagents were obtained from commercial suppliers and used without further purification.

2.2. Preparation of catalysts

2.2.1. Preparation of glucose phosphate carbamide (GluPC). Glucose was mixed with concentrated phosphoric acid and urea to make a homogeneous paste. The molar ratio of the three reagents was $1:2:6$. Then the mixture was transferred to an oven that had been heated to 135 °C for 2 h. After cooling to room temperature, the mixture was dissolved by the addition of deionized water. Methanol was added to precipitate the product from the aqueous phase. Finally, the product (GluPC) was collected and washed with 80% (v/v) aqueous methanol (20 mL × 3) and methanol (20 mL × 1), and dried at 60 °C in a vacuum for 8 h.

2.2.2. Preparation of the GluPC-zirconium complex (GluPC-Zr). In a typical procedure, GluPC (0.5 g) and $ZrCl_4$ (0.75 g) were respectively dissolved in 8 mL and 10 mL of water to obtain GluPC and $ZrCl_4$-derived sol solutions under ultrasound for 5 min, respectively, as supported by the dynamic light scattering results of these two aqueous solutions (see Fig. S1, ESI†). Subsequently, these two sol solutions were mixed and stirred with a magnetic stirrer at room temperature for 30 min. Afterwards, the mixture was transferred into a Teflon-lined stainless-steel autoclave (25 mL) and tightly sealed. The autoclave was placed into an oven that had been heated to 120 °C. After 12 h of hydrothermal reaction, the autoclave was taken out and cooled to room temperature. The obtained brown precipitates were filtered, and washed with distilled water and ethanol (10 mL × 3) until the filtrate became colorless and neutral (pH = 7). The obtained solid was dried at 60 °C in a vacuum for 12 h to afford about 0.8 g of GluPC-Zr complex.

2.3. Characterization

Transmission FT-IR spectra of the samples from 400 to 4000 cm^{-1} were recorded on a Nicolet Nexus 510 P FT-IR spectrometer using a KBr disk. Pyridine adsorbed FT-IR spectra of the catalyst were obtained on Tensor 27 equipment using KBr pellets in the range of 400–4000 cm^{-1} to determine the types of acid sites. The amount of Brønsted acid sites was calculated according to the 1545 cm^{-1} characteristic band and the amount of Lewis acid sites was calculated according to the 1445 cm^{-1} characteristic band. N_2 adsorption–desorption isotherms of the samples were measured at liquid nitrogen temperature using a Tristar 3000 fully automatic surface area and pore analyzer. Before testing, all the samples were degassed at 200 °C for 5 h. X-ray diffraction (XRD) measurements of the samples were conducted on an X-ray diffractometer (Ultima IV, Japan) operated at 40 kV and 250 mA with Cu Kα (λ = 0.15406 nm) radiation. The thermal stability of the samples was examined using thermogravimetric analysis (TGA)

(NETASCH, STA409PC) at a temperature from 25 to 960 °C under flowing N_2 (heating rate of 20 °C min^{-1}). X-ray photoelectron spectroscopy (XPS) of the samples was measured on a VG Multi Lab 2000 system with a monochromatic Mg-Kα source operated at 20 kV. Transmission electron microscopy (TEM) images of the samples were obtained from a JEOL JEM-2100 transmission electron microscope at an accelerating voltage of 200 kV. The sample for TEM analysis was dispersed in ethanol with the aid of sonication and then dropped onto a copper grid-supported carbon film. The zirconium and phosphorus contents were determined with ICP-OES equipment (PerkinElmer 8300). The particle size distribution of the sample in aqueous solution was measured on a Nano ZS90 dynamic light scattering device with a He–Ne laser (at λ = 633 nm) as the light source and an instrument power of 75 mW.

2.4. CTH reaction operation

In a typical CTH reaction operation, LA or its ester (5 mmol, 0.58 g), IPA (35 mmol, 2.67 mL) and GluPC-Zr (0.05 g) were mixed in a 10 mL Teflon-lined stainless-steel autoclave and magnetically stirred for 10 min to obtain a very stable brown suspension (see Fig. S2†). Then, the reactor was transferred into an preheated oven and the suspension was reacted at 180 °C for 12 h. The comparative data of reactions under stirring and without stirring listed in Table S1† indicated that this pseudo-homogeneous reaction does not seem to need stirring. After the reaction, the cooled mixture was centrifuged to collect the filtrate for the analysis of the products. The quantification of products was conducted on a gas chromatograph (GC, Shimadzu GC-2010) equipped with an FID detector and HP-5 capillary column (30.0 m × 250 mm × 0.25 mm) using dodecane as the internal standard. The identification of the products was done by GC-MS (Shimadzu QP2010).

2.5. Leaching experiments

After 2 h of the above-mentioned CTH reaction, the catalyst was filtered out from the reaction system and the collected filtrate was allowed to react for another 10 h under identical conditions to assess the leaching of the catalyst.

2.6 Catalyst recycling experiments

The recycling test of GluPC-Zr was performed as follows: after the reaction had proceeded at 180 °C for 12 h, the used GluPC-Zr was separated from the reaction mixture by centrifugation and washed with IPA until the filtrate was colorless, and then further washed with absolute ethanol (10 mL × 3). After drying at 60 °C under vacuum for 12 h, the recovered GluPC-Zr was directly employed for the next cycle under identical reaction conditions.

3. Results and discussion

3.1. Characterization results of samples

3.1.1. Elemental analysis. The main active elements of samples were measured by inductively coupled plasma (ICP)

analysis and the obtained data are listed in Table S2.† The P content of GluPC is up to 17.6 wt%, indicating that glucose can be well functionalized by phosphoric acid under the treatment conditions described in the Experimental section. The P and Zr contents of GluPC-Zr measured by ICP are 7.2 and 13.6 wt%, respectively, showing that GluPC can well coordinate with the Zr^{4+} sol to form a hybrid catalyst.

3.1.2. Functional groups and acidity. Fig. 1A gives the FT-IR spectra of glucose, GluPC and GluPC-Zr. The IR spectrum of glucose shows its characteristic absorption bands in the range 3500–400 cm^{-1}. After glucose turns into a GluPC ligand, its OH stretching vibration band at 3420 cm^{-1} decreases remarkably and its C–H bond stretching vibration bands in the range 2950–2890 cm^{-1} nearly disappear, along with the generation of some new IR absorption bands. These

new bands are assigned to the stretching vibrations of various hydrophilic groups, including NH_2 at 3184 cm^{-1}, COOH at 1710 cm^{-1}, $CONH_2$ at 1632 cm^{-1}, Ar–OH at 1610 cm^{-1} and polycyclic aromatics in the range 1400–1600 cm^{-1},[62] indicating that glucose is likely to be dehydrated to form the soluble CQD with the above hydrophilic groups attached under co-treatment with phosphoric acid and urea at 135 °C, consistent with the UV-vis and PL spectra of GluPC in Fig. S3.† Notably, two IR bands at 1054 and 926 cm^{-1} can also be found in the FT-IR spectrum of GluPC, a strong band at 1054 cm^{-1} is attributed to the symmetrical vibration of P=O in polyphosphate (P=OOH) or the C–O–P bond in the P-containing carbonaceous species[63] and another weak band at 926 cm^{-1} is assigned to the stretching vibration of the P–O–P bond.[64] This indicates the incorporation of polyphosphate groups and the
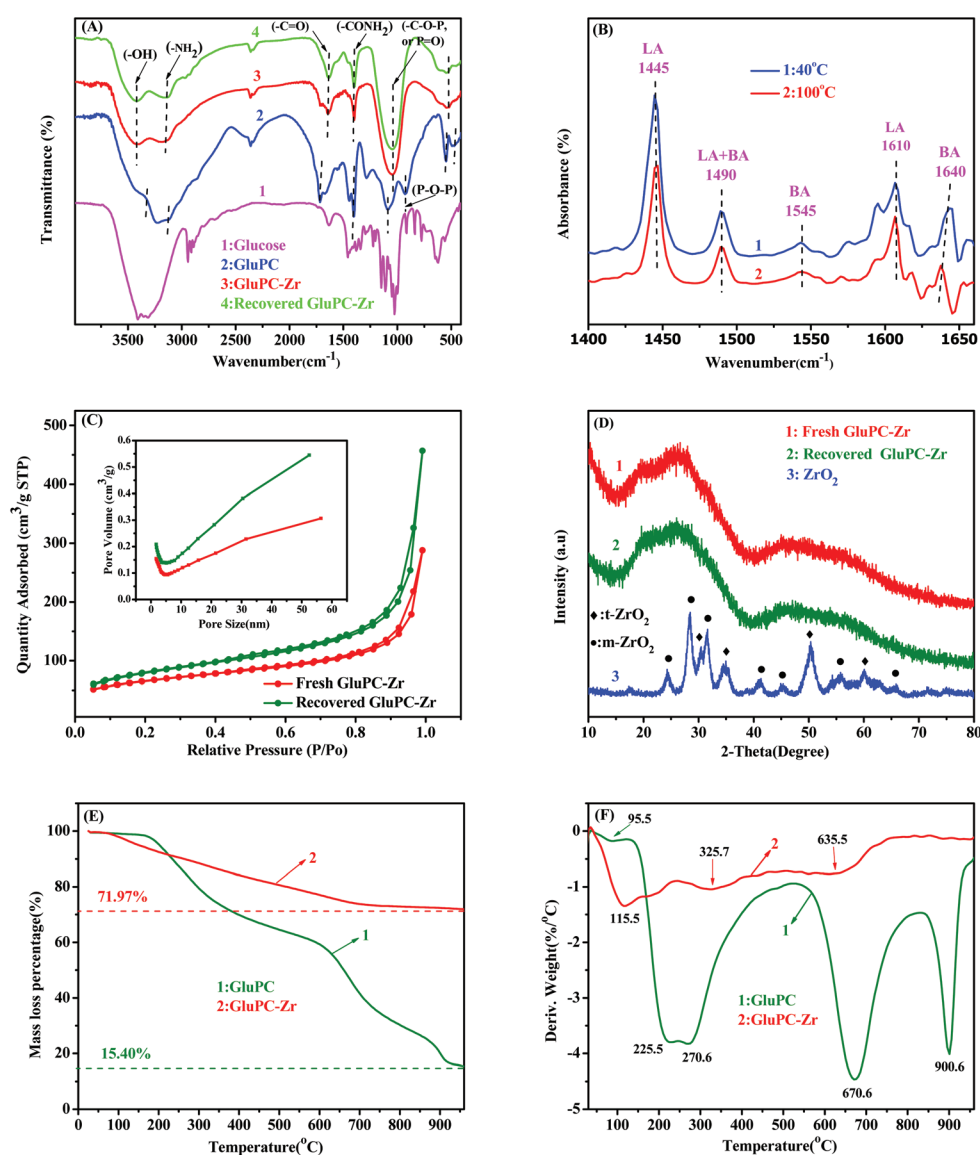

Fig. 1 FT-IR spectra (A), pyridine-adsorbed FT-IR spectra of GluPC-Zr (B), N_2 adsorption–desorption isotherms and BJH pore size distributions (C), powder XRD patterns (D), and thermogravimetric (E) and differential DTG (F) curves of samples.

P-containing carbonaceous species in the GluPC ligand, as supported by the ICP analysis of GluPC. After treatment with the Zr^{4+} sol, the above IR bands attributable to the ligand undergo different degrees of blue-shift and the COOH band becomes strong, along with a decrease in the $CONH_2$ band and the disappearance of the P–O–P band. These changes in the FT-IR spectrum of GluPC-Zr show that the Zr^{4+} sol can coordinate with all the hydrophilic groups of GluPC to form a hybrid catalyst containing Zr and P active species, as supported by ICP analysis. On the other hand, the strong acidity of the aqueous medium caused by $ZrCl_4$ hydrolysis is likely to lead to the hydrolysis of $CONH_2$ into COOH groups and the cleavage of the P–O–P bond in the polyphosphates during the hydrothermal preparation of GluPC-Zr.

In order to examine the acidity of GluPC-Zr, pyridine-adsorbed FT-IR spectra were conducted at two desorption temperatures of 40 and 100 °C under vacuum conditions. As shown in Fig. 1B, five IR bands at 1445, 1490, 1545, 1610 and 1640 cm^{-1} are found in the pyridine-adsorbed FT-IR spectra, and they are assigned to the pyridine adsorbed on the Lewis acidic (LA) sites, on the Brønsted acidic (BA) sites or both of these two acid sites in GluPC-Zr.[65,66] The LA and BA sites in GluPC-Zr should mainly originate from the Zr^{4+} centers and the P-containing functional groups, respectively. Also, the BA and LA sites were quantified according to 1545 and 1445 cm^{-1} characteristic bands and the calculated data are listed in Table S3.† At 40 °C, the LA amount of GluPC-Zr is 0.309 mmol g^{-1}, and it is much higher than the amount of BA (0.059 mmol g^{-1}), in line with the above ICP data. Raising the degassing temperature to 100 °C results in a decrease in these two acid amounts to 0.198 and 0.053 mmol g^{-1}, respectively. Notably, the rate of reduction in the amount of BA (about 10%) is much lower than that in the amount of LA (about 36%). These findings indicate that the strong B acidity and high LA sites of GluPC-Zr should be advantageous to the pre-esterization and CTH reactions of LA with IPA, respectively.

3.1.3. Porosity. The porosity of the GluPC-Zr sample was measured using a low-temperature nitrogen (N_2) adsorption apparatus and the obtained N_2 adsorption–desorption isotherms are shown in Fig. 1C. There, the isotherm of GluPC-Zr belongs to type II according to the IUPAC classification. At low to moderate relative pressures (0–0.8), the isotherm shows very slow increase in N_2 uptake without hysteresis. At high relative pressure, the isotherm exhibits a fast increase in N_2 uptake with type H3 narrow and inconspicuous hysteresis, which can be indicative of the characteristics of slit-shaped mesopores and macropores.[67] The inset in Fig. 1C displays that the BJH pore size distribution curve of GluPC-Zr presents a typical hierarchical pore character that consists of mesopores smaller than 5 nm and meso–macropores more than 5 nm. The porous parameters listed in Table S4† further reveal that GluPC-Zr has good porosity and its BET surface area (S_{BET}/m² g^{-1}), total pore volume (V_p/cm³ g^{-1}) and average porous size (D/nm) are 224, 0.4 and 10.9, respectively, and the ratio of its t-plot surface area (175 m² g^{-1}) is up to 78%, further indicating that the porosity of GluPC-Zr mainly originates from the con-

tribution of slit-shaped pores. These findings suggest that GluPC-Zr has richer hierarchical slit-shaped pores that can improve the diffusion of substrate and its accessibility to the active sites in the pores.

3.1.4. XRD. Fig. 1D shows the XRD patterns of commercial ZrO_2 and GluPC-Zr samples. There, some characteristic diffraction peaks in the range 20–60° are observed in the XRD pattern of ZrO_2, among them, four diffraction peaks at 30.4, 35, 50.4 and 60.2° are attributable to the tetragonal crystal (t-ZrO_2) and six other diffraction peaks at 24.2, 28.4, 31.6, 41.4, 45.3 and 55.8° are assigned to the monoclinic crystal (m-ZrO_2),[68,69] indicating that ZrO_2 is a mixture of tetragonal and monoclinic phases. GluPC-Zr presents two very broad diffraction bands in the range 15–60° in the XRD pattern. A strong broad peak in the range 10–40° (centered 2θ of 25.8°) is assigned to amorphous carbon composed of aromatic carbon sheets oriented in a random fashion,[70] another weak broad peak in the range 40–60° is attributable to the a-axis of the graphite structure,[71,72] which can be indicative of the CQD character of its ligand. But its XRD pattern lacks the above characteristic diffraction peaks of crystalline ZrO_2, suggesting that the initial small nucleated ZrO_2 particles (1.5–4.8 nm, see Fig. S1B†) obtained by the hydrolysis of $ZrCl_4$ solution can be well maintained in the hybrid catalyst through strong coordination with GluPC, and which show a significant diffraction peak broadening.

3.1.5. TGA. The thermal decomposition behaviors of GluPC and GluPC-Zr were checked via the thermogravimetric analysis (TGA) technique and the obtained TG and its differential (DTG) curves are depicted in Fig. 1E and F. The DTG curve of GluPC displays five weight-loss peaks in the range 90–1000 °C; among these weight-loss peaks, the first weak peak at 96 °C corresponds to evaporation of the adsorbed water molecules. Two unseparated strong peaks at 226 and 271 °C are likely to originate from the decomposition of the hydrophilic OH, NH_2, COOH and $CONH_2$ groups of GluPC, and the fourth strong peak at 671 °C may be attributed to the further carbonization process of carbonaceous species and the last peak at 901 °C is perhaps related to the decomposition of the incorporated polyphosphates. The P-containing residual species is estimated to be ca. 15.4 wt% based on the TG curve of GluPC, which is slightly lower than the P content (17.6 wt%) measured by ICP analysis. Compared to GluPC, the weight-loss peak for the adsorbed water molecules becomes strong and shifted to 116 °C in the DTG curve of GluPC-Zr, indicating that this porous material has a strengthened adsorption capacity for water. In addition, the decomposition peaks for the hydrophilic groups of the ligand become significantly weak and shifted toward high temperature in the DTG curve of GluPC-Zr, further affirming the strong coordination between GluPC and the Zr sol. Notably, the above-mentioned decomposition peak at 900 °C is not found in the DTG curve of GluPC-Zr, suggesting that the incorporated polyphosphates may be converted into very stable zirconium phosphate salts by the reaction with the Zr^{4+} sol under hydrothermal conditions, as supported by up to 72 wt% of inorganic species in GluPC-Zr by TGA analysis.

3.1.6. XPS. X-ray photo-electron spectroscopy (XPS) was used to investigate the chemical states for the surface atoms of GluPC and GluPC-Zr and the recorded high resolution XPS spectra for the surface Zr, O, P and N atoms are shown in Fig. 2. The survey spectra in Fig. S4A† affirm the existence of C, O, P and N elements in these two samples, as well as the existence of Zr element in GluPC-Zr. The deconvoluted high resolution XPS spectra for the surface C, O, P and N atoms by Gaussian simulation support the existence of various hydrophilic groups described in the FT-IR spectrum of GluPC (see Fig. S4C–F†). Fig. 2A–C show that the binding energies of O 1s, P 2p and N 1s for GluPC appear at 531.98, 133.23 and 399.58 eV, respectively. The introduced Zr species results in a slight decrease in O 1s binding energy to 531.58 eV and an increase in P 2p and N 1s binding energies to 133.78 and 400.23 eV. And the high resolution XPS spectrum for the surface C atoms of these two samples also displays that two C 1s energy bands in GluPC are shifted to slightly higher energy levels after introducing the Zr species (Fig. S4B†). Fig. 2D shows that the Zr 3d spectrum of GluPC-Zr exhibits two energy bands at 183.08 and 185.38 eV, which are attributable to Zr $3d_{5/2}$ and Zr $3d_{3/2}$,[66] respectively, and these two bands become shifted to higher energy levels compared to the previously reported high resolution XPS spectrum of Zr 3d in ZrO_2 (182.2 and 184.6 eV).[50] These findings confirm that the coordination between the hydrophilic groups of GluPC and the Zr^{4+} sol can bestow GluPC-Zr with the enhanced Lewis acidic Zr^{4+} and basic O^{2-} sites that are more beneficial to activating the carbonyl groups

in LA and disaggregating the hydroxyl groups in IPA, respectively, and the efficient synergy of these two types of active sites should significantly accelerate the CTH reaction of LA and its esters.

3.1.7. TEM. The morphologies of GluPC and GluPC-Zr were observed on a TEM instrument and the obtained images are shown in Fig. 3. In the TEM image of GluPC, its nanoparticles (NPs) are mostly between 5 and 15 nm, presenting a very loosely aggregated shape. The TEM image of GluPC-Zr presents a cage-like structure connected by various sizes of blocky particles and its large blocky surface attaches some NPs, suggesting that the coordination between GluPC and the Zr^{4+} sol can assemble into a network structure.

3.2 Catalytic performance evaluation

3.2.1 CTH reaction of LA with IPA. Table 2 lists the comparative data for the CTH reactions of LA with IPA catalyzed by GluPC-Zr and commercial zirconium compounds. As expected, the ligand GluPC is not active for the CTH reaction (entry 1). Among the examined zirconium compounds, $Zr(SO_4)_2$ does not have any activity for this CTH reaction although it can catalyze the esterification of LA with IPA (13.1% isopropyl levulinate (IPL) yield, entry 2). $Zr(OH)_4$ and ZrO_2, due to severe deactivation at high LA concentrations,[73] show poor activities for the reaction and achieve only 8.6 and 13.6% γ-GVL yields, respectively, along with the formation of a large amount of esterified product IPL (entries 3 and 4). $ZrOCl_2$ and $ZrCl_4$ achieve medium 49.7 and 58% γ-GVL yields in the CTH reac-
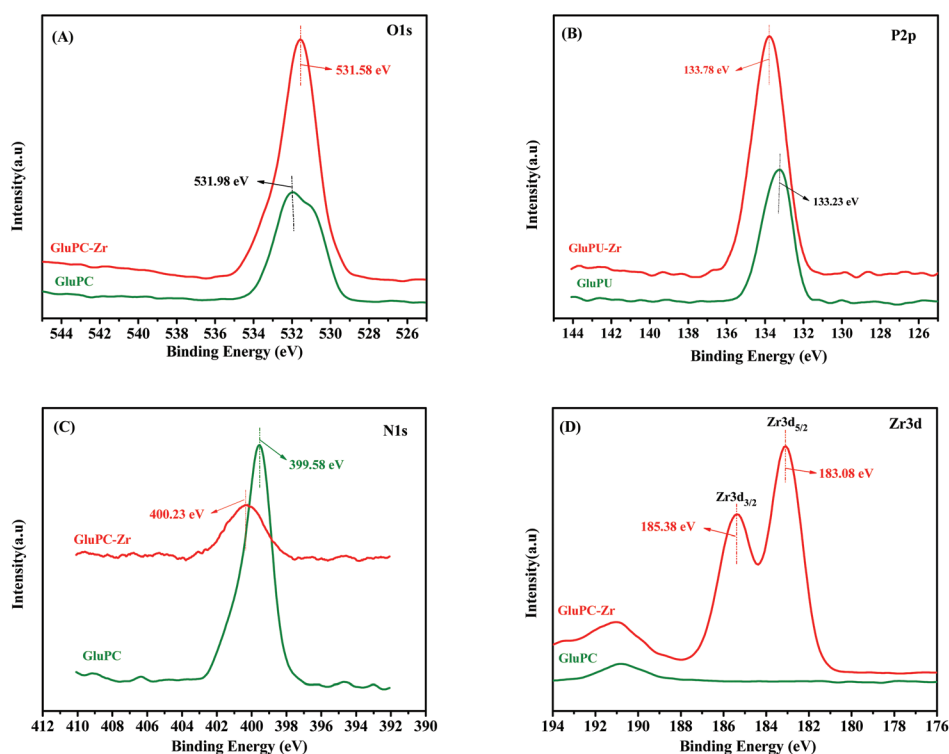

Fig. 2 High resolution XPS spectra of GluPC and GluPC-Zr: (A) O 1s XPS spectra; (B) P 2p XPS spectra; (C) N 1s XPS spectra; and (D) Zr 3d XPS spectra.
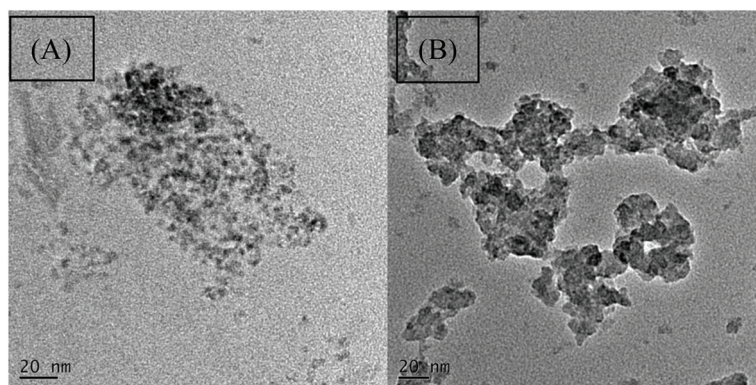
Fig. 3 TEM images of GluPC (A) and GluPC-Zr (B).

Table 2 CTH reaction of LA with IPA over various Zr-based catalysts[a]

Entry	Catalyst	T (°C)	Time (h)	Conversion (%)	Yield of γ-GVL (%)	Yield of IPL (%)	TOF (mmol g^{-1} h^{-1})
1	GluPC	180	12	—	—	—	—
2	Zr(SO$_4$)$_2$	180	12	13.1	0	13.1	0
3	ZrO$_2$	180	12	73.1	8.2	64.9	0.7
4	Zr(OH)$_4$	180	12	86.6	13.6	73	1.1
5	ZrCl$_4$	180	12	100	49.7	49.3	4.1
6	ZrOCl$_2$	180	12	100	58.0	41.0	4.8
7	GluPC-Zr	180	12	100	95	1.99	7.9
8	GluPC-Zr	190	12	100	98.1	0.88	8.2
9	GluPC-Zr	150	12	100	83.7	14.7	7.0
10	GluPC-Zr	150	20	100	92.6	5.9	4.6
11[b]	GluPC-Zr	150	10	100	95.1	3.1	1.9
12	GluPC-Zr	120	12	98.1	46.2	51.3	3.9

[a] Reaction conditions: GluPC-Zr, 0.05 g; LA, 5 mmol; IPA, 35 mmol. [b] LA, 1 mmol.

tion of LA but still nearly half of the IPL cannot be converted into γ-GVL (entries 5 and 6). Inspiringly, GluPC-Zr can tolerate a high LA concentration (1.87 M) and achieve up to 95% γ-GVL yield at a relatively low catalyst dosage (0.05 g, about 8.6 wt% relative to LA), providing 7.9 turnover frequency (TOF/mmol γ-GVL per g catalyst per h, entry 7). The TOF value of GluPC-Zr further increases to 8.2 at 190 °C, giving the highest 98.0% γ-GVL yield (entry 8). But the TOF value is slightly reduced to 7.0 at a lower temperature of 150 °C (entry 9), but prolonging the reaction time to 20 h also achieves 92.6% γ-GVL yield (entry 10). In addition, when LA is reduced to 1 mmol, the reaction temperature and time to achieve a higher than 95% γ-GVL yield over GluPC-Zr are reduced to 150 °C and 10 h, respectively (entry 11). When the temperature is further reduced to 120 °C, LA conversion can still be up to 98.1%, but its esterified product IPL yield (51.3%) is higher than that of γ-GVL (46.2%, entry 12), confirming that the P-containing Brønsted acidic sties of GluPC-Zr are likely to preferentially catalyze the esterification of LA with IPA. Compared to the CTH catalysts previously reported in the literature, the current GluPC-Zr may be easily synthesized at large scale and low cost by simple two-step conversion, but it can also work well at high LA concentration like a benchmark ruthenium catalyst,

showing a much higher catalytic efficiency than the other Zr-based catalysts listed in Table 1.

3.2.2 Effects of various variables. The effect of various variables, such as catalyst dosage, IPA/LA molar ratio, reaction temperature and time on the TH reaction of LA catalyzed GluPC-Zr was further investigated using IPA as a hydrogen donor and the results are depicted in Fig. 4. There, LA conversion is insensitive to the change in these variables and can remain higher than 99%. γ-GVL yield continuously increases with an increase in these variables, along with a gradual decrease in the esterified product IPL. The highest 98.1% γ-GVL yield can be obtained under the optimal variables (0.05 g catalyst, IPA/LA molar ratio of 7, 190 °C, 12 h). Notably, when any one of these variables is at its lowest level, a non-ignorable amount of IPL is produced under these reaction conditions. These findings suggest that GluPC-Zr can preferentially and rapidly catalyze the esterification of LA with IPA to IPL, and its inherent CTH performance may be retained by the preferential esterification strategy of LA, thus showing an excellent catalytic efficiency in the conversion of a high concentration of LA to γ-GVL.

3.2.3 Influence of the hydrogen donor on the CTH reaction of LA. The effect of secondary alcohols on the GluPC-Zr-cata-
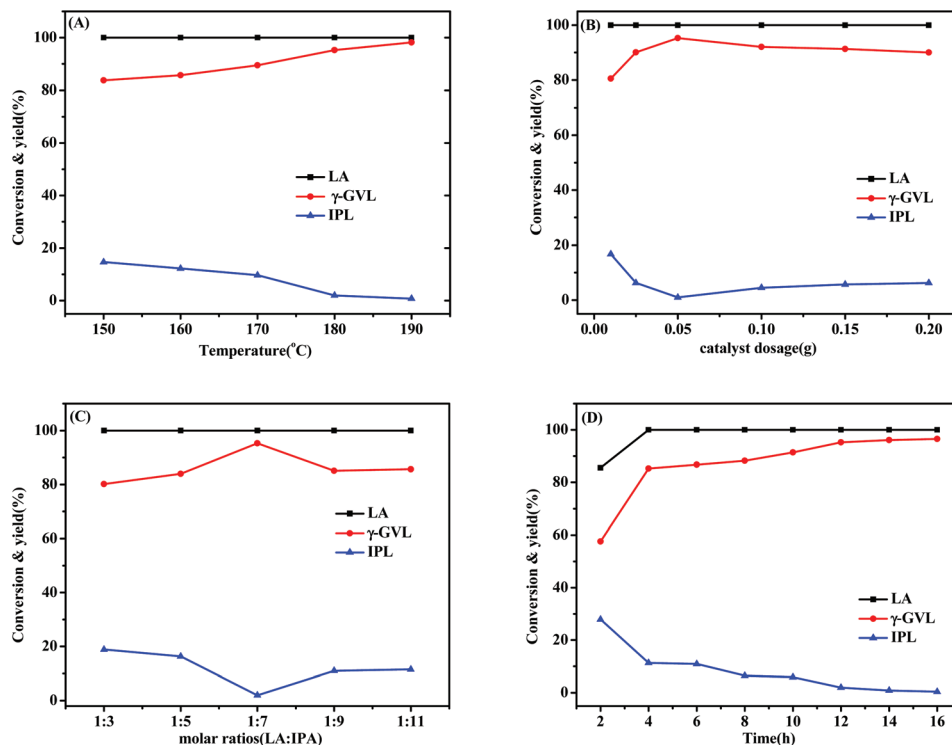
Fig. 4 The influence of the reaction temperature (A), catalyst dosage (B), LA/IPA molar ratio, (C) and reaction time (D) on the GluPC–Zr-catalyzed TH reaction of LA with IPA. (Using the same reaction conditions as in entry 7 of Table 2, except for the studied variable.)

lyzed conversion of LA to γ-GVL was investigated and the results are depicted in Fig. 5A. Among the secondary alcohols examined, IPA is an excellent hydrogen donor, providing 100% LA conversion with 95% γ-GVL yield. 2-Butanol, 3-pentanol, and cyclohexanol exhibit obviously low efficiency as hydrogen donors, giving only 65, 52 and 66% γ-GVL yields, respectively, which is likely to be due to the following reasons. The pre-esterification rate of LA is inversely proportional to the carbon chain length of the secondary aliphatic alcohol[74] and its toxic effect on the catalyst easily occurs upon 2-butanol and especially 3-pentanol, as supported by the following facts. In the presence of these two alcohols, about 5% of LA is not con-

verted. On the other hand, the hydrogen transfer rate of secondary alcohol to the transition product ester is influenced by the steric effect of the ester, which is most obvious when cyclohexanol is used as the hydrogen donor. Cyclohexanol easily reacts with LA (100% LA conversion) but its derived ester is not easily converted into γ-GVL, owing to the serious steric effect.

3.2.3 CTH reaction of levulinate esters. The CTH performance of GluPC-Zr was tested with methyl levulinate (ML), ethyl levulinate (EL), isopropyl levulinate (IPL) and butyl levulinate (BL) instead of LA under the same reaction conditions and the results are shown in Fig. 5B. It can be seen from Fig. 5B that
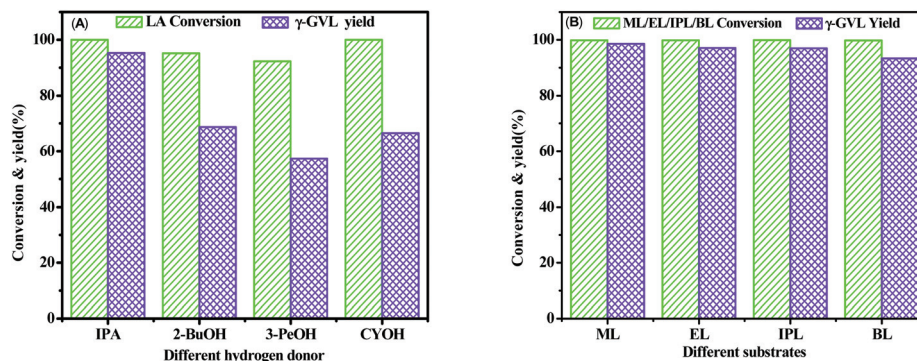

Fig. 5 The effects of hydrogen donors on the CTH reaction of LA (A) and a comparison of the CTH reactions of LEs with IPA (B). (Reaction conditions: LA/LEs, 5 mmol; GluPC–Zr, 0.05 g; alcohol, 35 mmol; 180 °C; 12 h.)
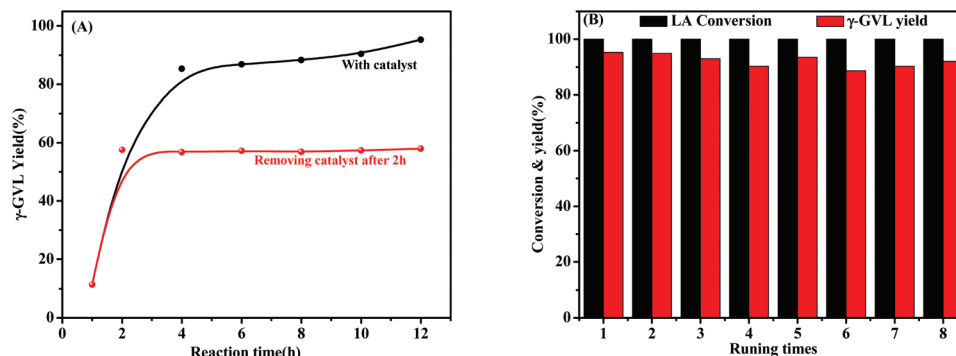
Fig. 6   Heterogeneity (A) and reusability (B) of the GluPC–Zr catalyst in CTH reactions of LA with IPA.

the conversions of these levulinate esters are all close to 100%, and the yields of γ-GVL are higher than 93%, which are considerable compared with LA. Among the esters examined, ML is the most active, providing the highest 98% γ-GVL yield. EL and IPL as the substrates also achieve excellent 97% γ-GVL yield. While the reactivity of BL slightly declines as the increase of alkyl carbon chain causes the lactonization of the hydrogen transfer-derived intermediate 4-hydroxy alkyl levulinate become relatively difficult,[75] giving a slightly low 93% γ-GVL yield.

3.2.5   Heterogeneity and recycling experiments. In order to confirm that the CTH reaction of LA with IPA is heterogeneous, the reaction catalyzed by GluPC-Zr proceeded for 2 h at 180 °C and then the solid catalyst was filtered from the reaction solution, and the resulting filtrate was allowed to react for another 10 h under identical conditions and the obtained result is shown in Fig. 6A. There, this heterogeneous catalysis reaction can achieve 57% γ-GVL yield after 2 h but the filtering to remove the solid catalyst does not give any extra increase in γ-GVL yield in the following reaction for 10 h, indicating that the solid catalyst is very stable and the leaching of its active species does not occur during the reaction, which can be further confirmed by the following recycling experiments of CTH reactions of LA and ML. As shown in Fig. 6B and Fig. S5,† in seven consecutive reaction cycles, the conversions of LA and ML all remain constant at 100%, and the yield of γ-GVL shows only an inappreciable decrease. The GluPC-Zr recovered after the seventh run was characterized by FT-IR, BET and XRD methods and the results indicated that the recovered catalyst has almost the same characteristic IR absorption bands and XRD patterns as the fresh sample (Fig. 1A and D), it still retains good porosity (Fig. 1C) and its porous parameters ($S_{t\text{-plot}}$, V_p and D values) have improved to some extent (Table S4†). We suggest that the strong interaction of GluPC-Zr with the alcohol solvent, as supported by Fig. S2,† may make the aggregation of catalyst particles become slightly looser during the CTH reaction run, thus increasing the number and size of slit-shaped pores constructed by recovered catalyst particles. These findings confirm that the strong coordination between GluPC and the Zr^{4+} sol can bestow the catalyst with a very stable framework, active sites, and pores,

thus showing excellent reusability in the CTH reactions of LA and ML.

4.   Conclusions

In conclusion, for the first time we have constructed an excellent and recyclable GluPC-Zr catalyst for the CTH reactions of levulinic acid (LA) or its esters, which has the following advantages: (i) two raw materials, glucose and $ZrCl_4$, for the preparation of the catalyst are inexpensive and readily available, and the catalyst is easily synthesized at large scale and low cost *via* simple two-step conversion; (ii) GluPC-Zr has outstanding CTH performance and excellent reusability, and it can achieve the almost quantitative conversion of a high concentration of LA to γ-GVL at catalytic amounts, exhibiting much superior catalytic efficiency to previously reported Zr-based catalysts. This low-cost, environmentally benign, and recyclable catalyst is highly desirable to realize the large-scale production of γ-GVL from biomass-derived LA. In the future, we are interested in constructing GluPC-mediated bimetallic catalysts to realize one-pot conversion from carbohydrates to γ-GVL.

Conflicts of interest

The authors declare that they have no known competing financial interests or personal relationships that could have appeared to influence the work reported in this paper.

Acknowledgements

References

1 E. L. Kunkes, D. A. Simonetti, R. M. West, J. C. Serrano-Ruiz, C. A. Gärtner and J. A. Dumesic, *Science*, 2008, **322**, 417–421.

2 L. C. H. Chow, *Eurasian Geogr. Econ.*, 2011, **52**, 523–528.

3 G. W. Huber, S. Iborra and A. Corma, *Chem. Rev.*, 2006, **106**, 4044–4098.

4 A. Fukuoka and P. L. Dhepe, *Angew. Chem., Int. Ed.*, 2006, **45**, 5161–5163.

5 S.-S. Liu, K.-Q. Sun and B.-Q. Xu, *ACS Catal.*, 2014, **4**, 2226–2230.

6 P. Gallezot, *Chem. Soc. Rev.*, 2012, **41**, 1538–1558.

7 H. Hassan, J. K. Lim and B. H. Hameed, *Bioresour. Technol.*, 2016, **221**, 645–655.

8 A. Corma, S. Iborra and A. Velty, *Chem. Rev.*, 2007, **107**, 2411–2502.

9 M. J. Biddy, R. Davis, D. Humbird, L. Tao, N. Dowe, M. T. Guarnieri, J. G. Linger, E. M. Karp, D. Salvachúa, D. R. Vardon and G. T. Beckham, *ACS Sustainable Chem. Eng.*, 2016, **4**, 3196–3211.

10 H. Lin, J. Strull, Y. Liu, Z. Karmiol, K. Plank, G. Miller, Z. Guo and L. Yang, *Energy Environ. Sci.*, 2012, **5**, 9773–9777.

11 N. Armaroli and V. Balzani, *Angew. Chem., Int. Ed.*, 2007, **46**, 52–66.

12 P. S. Shuttleworth, M. De bruyn, H. L. Parker, A. J. Hunt, V. L. Budarin, A. S. Matharu and J. H. Clark, *Green Chem.*, 2014, **16**, 573–584.

13 M. M. Antunes, S. Lima, P. Neves, A. L. Magalhães, E. Fazio, F. Neri, M. T. Pereira, A. F. Silva, C. M. Silva, S. M. Rocha, M. Pillinger, A. Urakawa and A. A. Valente, *Appl. Catal., B*, 2016, **182**, 485–503.

14 Y. J. Pagán-Torres, T. Wang, J. M. R. Gallo, B. H. Shanks and J. A. Dumesic, *ACS Catal.*, 2012, **2**, 930–934.

15 H. Huang, C. A. Denard, R. Alamillo, A. J. Crisci, Y. Miao, J. A. Dumesic, S. L. Scott and H. Zhao, *ACS Catal.*, 2014, **4**, 2165–2168.

16 J. Guo, S. Zhu, Y. Cen, Z. Qin, J. Wang and W. Fan, *Appl. Catal., B*, 2017, **200**, 611–619.

17 S. E. Davis, B. N. Zope and R. J. Davis, *Green Chem.*, 2012, **14**, 143–147.

18 P. Carniti, A. Gervasini, F. Bossola and V. Dal Santo, *Appl. Catal., B*, 2016, **193**, 93–102.

19 S. Van de Vyver, J. Thomas, J. Geboers, S. Keyzer, M. Smet, W. Dehaen, P. A. Jacobs and B. F. Sels, *Energy Environ. Sci.*, 2011, **4**, 3601–3610.

20 S. Song, L. Di, G. Wu, W. Dai, N. Guan and L. Li, *Appl. Catal., B*, 2017, **205**, 393–403.

21 L. Bui, H. Luo, W. R. Gunther and Y. Román-Leshkov, *Angew. Chem., Int. Ed.*, 2013, **52**, 8022–8025.

22 J. Q. Bond, D. M. Alonso, D. Wang, R. M. West and J. A. Dumesic, *Science*, 2010, **327**, 1110–1114.

23 J.-P. Lange, R. Price, P. M. Ayoub, J. Louis, L. Petrus, L. Clarke and H. Gosselink, *Angew. Chem., Int. Ed.*, 2010, **49**, 4479–4483.

24 S. De, B. Saha and R. Luque, *Bioresour. Technol.*, 2015, **178**, 108–118.

25 X. Tang, X. Zeng, Z. Li, L. Hu, Y. Sun, S. Liu, T. Lei and L. Lin, *Renewable Sustainable Energy Rev.*, 2014, **40**, 608–620.

26 S. Song, S. Yao, J. Cao, L. Di, G. Wu, N. Guan and L. Li, *Appl. Catal., B*, 2017, **217**, 115–124.

27 I. T. Horváth, *Green Chem.*, 2008, **10**, 1024–1028.

28 X. Gao, S. Zhu, M. Dong, J. Wang and W. Fan, *Appl. Catal., B*, 2019, **259**, 118076.

29 Z.-P. Yan, L. Lin and S. Liu, *Energy Fuels*, 2009, **23**, 3853–3858.

30 L. Deng, Y. Zhao, J. Li, Y. Fu, B. Liao and Q.-X. Guo, *ChemSusChem*, 2010, **3**, 1172–1175.

31 L. E. Manzer, *Appl. Catal., A*, 2004, **272**, 249–256.

32 X. Du, Y. Liu, J. Wang, Y. Cao and K. Fan, *Chin. J. Catal.*, 2013, **34**, 993–1001.

33 W. Luo, M. Sankar, A. M. Beale, Q. He, C. J. Kiely, P. C. Bruijnincx and B. M. Weckhuysen, *Nat. Commun.*, 2015, **6**, 6540.

34 L. E. Manzer, *Appl. Catal., A*, 2004, **272**, 249–256.

35 X.-L. Du, L. He, S. Zhao, Y.-M. Liu, Y. Cao, H.-Y. He and K.-N. Fan, *Angew. Chem., Int. Ed.*, 2011, **50**, 7815–7819.

36 X. L. Du, Q. Y. Bi, Y. M. Liu, Y. Cao and K. N. Fan, *ChemSusChem*, 2011, **4**, 1838–1843.

37 O. A. Abdelrahman, A. Heyden and J. Q. Bond, *ACS Catal.*, 2014, **4**, 1171–1181.

38 K. Yan, T. Lafleur, G. Wu, J. Liao, C. Ceng and X. Xie, *Appl. Catal., A*, 2013, **468**, 52–58.

39 F. M. Geilen, B. Engendahl, A. Harwardt, W. Marquardt, J. Klankermayer and W. Leitner, *Angew. Chem., Int. Ed.*, 2010, **49**, 5510–5514.

40 C. Ortiz-Cervantes and J. J. García, *Inorg. Chim. Acta*, 2013, **397**, 124–128.

41 W. Li, J.-H. Xie, H. Lin and Q.-L. Zhou, *Green Chem.*, 2012, **14**, 2388–2390.

42 J. Deng, Y. Wang, T. Pan, Q. Xu, Q. X. Guo and Y. Fu, *ChemSusChem*, 2013, **6**, 1163–1167.

43 C. Ortiz-Cervantes, M. Flores-Alamo and J. J. García, *ACS Catal.*, 2015, **5**, 1424–1431.

44 H. Zhong, Q. Li, J. Liu, G. Yao, J. Wang, X. Zeng, Z. Huo and F. Jin, *ACS Sustainable Chem. Eng.*, 2017, **5**, 6517–6523.

45 A. M. Ruppert, M. Jędrzejczyk, N. Potrzebowska, K. Kaźmierczak, M. Brzezińska, O. Sneka-Płatek, P. Sautet, N. Keller, C. Michel and J. Grams, *Catal. Sci. Technol.*, 2018, **8**, 4318–4331.

46 A. M. Hengne, B. S. Kadu, N. S. Biradar, R. C. Chikate and C. V. Rode, *RSC Adv.*, 2016, **6**, 59753–59761.

47 Q. Xu, X. Li, T. Pan, C. Yu, J. Deng, Q. Guo and Y. Fu, *Green Chem.*, 2016, **18**, 1287–1294.

48 M. J. Gilkey and B. Xu, *ACS Catal.*, 2016, **6**, 1420–1436.

49 S. S. Enumula, V. R. B. Gurram, M. Kondeboina, D. R. Burri and S. R. R. Kamaraju, *RSC Adv.*, 2016, **6**, 20230–20239.

50 J. Song, B. Zhou, H. Zhou, L. Wu, Q. Meng, Z. Liu and B. Han, *Angew. Chem., Int. Ed.*, 2015, **54**, 9399–9403.

51 Z. Xiao, H. Zhou, J. Hao, H. Hong, Y. Song, R. He, K. Zhi and Q. Liu, *Fuel*, 2017, **193**, 322–330.

52 A. H. Valekar, K.-H. Cho, S. K. Chitale, D.-Y. Hong, G.-Y. Cha, U. H. Lee, D. W. Hwang, C. Serre, J.-S. Chang and Y. K. Hwang, *Green Chem.*, 2016, **18**, 4542–4552.

53 Z. Xue, J. Jiang, G. Li, W. Zhao, J. Wang and T. Mu, *Catal. Sci. Technol.*, 2016, **6**, 5374–5379.

54 Y. Xie, F. Li, J. Wang, R. Wang, H. Wang, X. Liu and Y. Xia, *Mol. Catal.*, 2017, **442**, 107–114.

55 J. Song, L. Wu, B. Zhou, H. Zhou, H. Fan, Y. Yang, Q. Meng and B. Han, *Green Chem.*, 2015, **17**, 1626–1632.

56 W. C. Yun, M. T. Yang and K. A. Lin, *J. Colloid Interface Sci.*, 2019, **543**, 52–63.

57 J. Wang, R. Wang, H. Zi, H. Wang, Y. Xia and X. Liu, *J. Chin. Chem. Soc.*, 2018, **65**, 750–759.

58 C. López-Aguado, M. Paniagua, J. A. Melero, J. Iglesias, P. Juárez, M. López Granados and G. Morales, *Catalysts*, 2020, **10**, 678.

59 C. Xie, J. Song, B. Zhou, J. Hu, Z. Zhang, P. Zhang, Z. Jiang and B. Han, *ACS Sustainable Chem. Eng.*, 2016, **4**, 6231–6236.

60 Z. Yu, X. Lu, C. Liu, Y. Han and N. Ji, *Renewable Sustainable Energy Rev.*, 2019, **112**, 140–157.

61 J. Wang, J. Liu, X. Yu, W. Zhang, G. Zhang, M. Liu, J. Shen, C. Yang and X. Jin, *Mater. Today Energy*, 2020, **18**, 100501.

62 B. Li, L. Zhou, D. Wu, H. Peng, K. Yan, Y. Zhou and Z. Liu, *ACS Nano*, 2011, **5**, 5957–5961.

63 A. M. Puziy, O. I. Poddubnaya, A. Martínez-Alonso, F. Suárez-García and J. M. D. Tascón, *Carbon*, 2002, **40**, 1493–1505.

64 S. Bourbigot, M. Le Bras, R. Delobel, P. Bréant and J.-M. Trémillon, *Carbon*, 1995, **33**, 283–294.

65 H. Li, T. Yang and Z. Fang, *Appl. Catal., B*, 2018, **227**, 79–89.

66 S. Zhou, F. Dai, Z. Xiang, T. Song, D. Liu, F. Lu and H. Qi, *Appl. Catal., B*, 2019, **248**, 31–43.

67 A. M. Puziy and O. I. Poddubnaya, *Carbon*, 1998, **36**, 45–50.

68 N. Shimoda, K. Nakayama, K. Kiyota and S. Satokawa, *RSC Adv.*, 2017, **7**, 55819–55829.

69 S. Zang, N. He, X. Sun, M. Sun, W. Wu and H. Yang, *Ceram. Int.*, 2019, **45**, 394–400.

70 M. Okamura, A. Takagaki, M. Toda, J. N. Kondo, K. Domen, T. Tatsumi, M. Hara and S. Hayashi, *Chem. Mater.*, 2006, **18**, 3039–3045.

71 J. Xi, Y. Zhang, Q. Xia, X. Liu, J. Ren, G. Lu and Y. Wang, *Appl. Catal., A*, 2013, **459**, 52–58.

72 S. Suganuma, K. Nakajima, M. Kitano, D. Yamaguchi, H. Kato, S. Hayashi and M. Hara, *J. Am. Chem. Soc.*, 2008, **130**, 12787–12793.

73 H. Kobayashi, H. Matsuhashi, T. Komanoya, K. Hara and A. Fukuoka, *Chem. Commun.*, 2011, **47**, 2366–2368.

74 W. Zhao, H. Ding, J. Zhu, X. Liu, Q. Xu and D. Yin, *J. Bioresour. Bioprod.*, 2020, **5**, 291–299.

75 A. M. Hengne and C. V. Rode, *Green Chem.*, 2012, **14**, 1064–1072.